Radiotherapeutic efficacy of gold nanoparticles for high dose-rate brachytherapy compared to conventional radiotherapy: An in vitro study

Daniel Cecchi, Nolan Jackson, Mehran Goharian, Wayne Beckham, and Devika Chithrani

2025

Original citation:
Cecchi, D., Jackson, N., Goharian, M., Beckham, W., & Chithrani, D. (2025). Radiotherapeutic efficacy of gold nanoparticles for high dose-rate brachytherapy compared to conventional radiotherapy: An in vitro study. *Medical Physics*, *52*(7), e18006. https://doi.org/10.1002/mp.18006

Received: 23 January 2025 | Revised: 25 June 2025 | Accepted: 29 June 2025

DOI: 10.1002/mp.18006

RESEARCH ARTICLE

MEDICAL PHYSICS

Radiotherapeutic efficacy of gold nanoparticles for high dose-rate brachytherapy compared to conventional radiotherapy: An in vitro study

Daniel Cecchi[1] | **Nolan Jackson**[1] | **Mehran Goharian**[1,2] | **Wayne Beckham**[1,2] | **Devika Chithrani**[1,2]

[1]Department of Physics and Astronomy, University of Victoria, Victoria, British Columbia, Canada

[2]British Columbia Cancer, Victoria, British Columbia, Canada

Correspondence
Devika Chithrani, Department of Physics and Astronomy, University of Victoria, Victoria, BC, Canada.
Email: devikac@uvic.ca

Funding information
NanoMedicines Innovation Network; Strategic Initiative, Grant/Award Number: 2021-RES-SI-05; Natural Sciences and Engineering Research Council (NSERC); Discovery Grant (DG), Grant/Award Number: RGPIN-2017-04501; Canadian Institutes of Health Research, Grant/Award Number: DC0190GP

Abstract

Background: Radiation therapy is a pivotal part of the treatment plan for many cancer patients. Effective dose escalation in the tumour is required to achieve optimal curative results but is hindered by normal tissue toxicity. Gold nanoparticles (GNPs) as radiosensitizers to improve the radiation cross-section of malignant tissue is one avenue currently being explored to improve therapeutic results. It is hypothesized that at lower incident photon energies, dose enhancement from GNPs should be significantly greater compared to high-energy irradiations due to a greater photoelectric cross-section.

Purpose: To assess GNP radiosensitization in vitro during low-energy, high-dose-rate brachytherapy (HDR-BT) irradiations and compare to the measured radiosensitization from a 6MV photon beam from a clinical linear accelerator (LINAC).

Methods: A novel Solid Water Phantom was developed for uniform irradiations from a common HDR-BT source (192-Ir) and verified using EBT-4 radiochromic film. HeLa (cervical) and PC3 (prostate) monolayer cell cultures were used to represent common HDR-BT treatment sites. The cells were dosed at 10 μg/mL concentration with functionalized 12 nm spherical GNPs. GNP uptake in the cellular membrane was quantified using live-cell imaging and a trace element analysis technique. Cell cultures with or without GNPs were irradiated from the 192-Ir source or clinical 6 MV photon beam from a LINAC to a 200 cGy dose prescription. Cellular viability was measured using a clonogenic assay and DNA double-strand break (DSB) assay.

Results: Endocytosis of spherical GNPs was confirmed 24 h post-incubation, resulting in an average of 8.7×10^5 GNPs/cell and 6.0×10^5 GNPs/cell for HeLa and PC3 cell cultures, respectively. The incorporation of GNPs induced 183% ($p < 0.001$) and 364% ($p = 0.01$) greater DNA DSBs with HDR-BT irradiations compared to LINAC irradiations for HeLa and PC3 cells, respectively, after the 200 cGy prescription. GNPs reduced the survival fraction of HeLa and PC3 cells after 2 weeks post-irradiation by 4.6% ($p < 0.05$) and 8.5% ($p < 0.05$), respectively, with HDR irradiations compared to LINAC irradiations.

Conclusions: Our results suggest GNP incorporation into HDR-BT is a viable and effective treatment strategy. As our dosing concentration in this study induced no measurable cellular toxicity, this strategy has the potential to

be implemented in clinical scenarios. Ultimately, we believe that incorporating GNPs into radiotherapy workflows can increase radiotherapeutic efficacy, improving the quality of life for cancer patients.

KEYWORDS
brachytherapy, cancer, nanoparticle, radiosensitizer, radiotherapy, therapeutics

1 | INTRODUCTION

Unavoidable normal tissue toxicity from current radiotherapy treatments greatly affects treatment viability and can significantly affect the patient's quality of life. With current radiotherapy practices like external beam radiotherapy or brachytherapy, the associated normal tissue complication probability can significantly limit effective dose escalation to the tumor (Figure 1a). To achieve dose escalation within the tumour, metal nanoparticles (NPs) as radiosensitizing agents are gaining interest as a viable technique to safely increase the dose to the tumour.[1] Throughout the past two decades, significant interest has been built for their effective implementation into clinical workflows, with Phase 1 clinical trials of novel metallic nanoparticles growing in popularity.[2,3] The primary function of metal NPs is to increase the photoelectric cross-section of malignant tissue, thereby generating a greater concentration of secondary electrons at the location of NP deposition. These secondary electrons have a short range (μm), depositing dose adjacent to the NPs or generating cell-damaging species such as free radicals. Their effective implementation into treatment plans can improve the therapeutic index, thereby reducing the probability of healthy tissue complications or enabling dose escalation in the tumour (Figure 1b). In pre-clinical research, gold nanoparticles (GNPs) are of particular interest due to their high-Z atomic structure (Z = 79), ease of production, and biocompatibility.[4–7] Due to gold's high photoelectric cross section ($\propto Z^3E^{-3}$), its potential for acting as a radiosensitizing agent has been reported extensively in the literature in a wide range of clinically relevant scenarios, including brachytherapy and high-energy external beam radiotherapy (EBRT).[4,8–10]

For effective GNP radiosensitization, treatments such as brachytherapy with radioactive sources emitting low to medium-energy photons may offer improved radiosensitization relative to high-energy EBRT.[11–13] Incident photons in the kilovoltage (keV) energy range interact predominantly through the photoelectric effect, resulting in a cascade of short-range secondary electrons. Meanwhile, high-energy megavoltage (MeV) incident photons interact primarily through the Compton effect, resulting in scattered photons that can carry a significant portion of their incident energy further away from the interaction site. Higher-energy radiation, indeed, leads to secondary electrons with greater penetration into surrounding tissue due to increased energy transfer. To this end, GNP-induced radiosensitization from clinical 6 MV photon beams is still reported in the literature.[14] One reason for this effect may be the inherent photon energy spectrum of clinical linear accelerators (LINACs), resulting in a reduction in the mean photon energy closer to 1.5–2 MeV and a significant proportion of keV photons. For effective local dose enhancement, lower keV photon energies are still the predominant choice of ionizing radiation. Many Monte Carlo (MC) studies evaluating GNP radiosensitization in high and low-energy regimes support this hypothesis – either regarding the generation of secondary electrons in the vicinity of the GNPs or by the dose enhancement to water.[15–18]

Extensive research has been conducted to integrate GNPs into brachytherapy treatments.[4,10,19–25] Low dose-rate (LDR) brachytherapy with GNPs can demonstrate greater dose enhancement with lower energy photons, but the conventionally long treatment duration makes it difficult to measure their effects in standard lab settings accurately. High-dose-rate (HDR)-brachytherapy (HDR-BT), characterized by high activity sources like 192-Ir (average emission energy of ~380 keV[26]) emitting mid-range energy photons, may offer more relevant applications for GNP radiosensitization. HDR-BT is commonly prescribed as adjuvant radiotherapy with EBRT for sites such as the cervix and prostate, offering a local boost to areas that require additional treatment. Initial Monte Carlo studies evaluating dose enhancement using 192-Ir showed significant radiosensitization between 1.04 and 2.0, dependent on the concentration of gold (0.2–100 mg Au/g of tumour).[27–29] In vitro studies on GNP incorporation into HDR-BT have also shown effective radiosensitization with varying GNP concentrations and sizes with an 192-Ir source. Shahhoseini et al.[24] reported a dose enhancement of 1.54 and 1.67 on lung and prostate cancer cell lines, respectively, with 15 nm GNPs dosed at approximately 21 nM (~20 mg/kg in vivo, assuming 2 mL of blood volume and 20 g bodyweight). Yogo et al.[25] also reported a dose-enhancement of 1.5 with DNA double-strand breaks from 1.4 nm positively-charged GNPs dosed at 64 ng/mL on plasmid DNA. While these results effectively demonstrate the efficacy of GNPs for radiosensitization, their applicability in clinical settings is limited due to relatively high concentrations of GNPs that may lead to toxicity concerns in vivo or

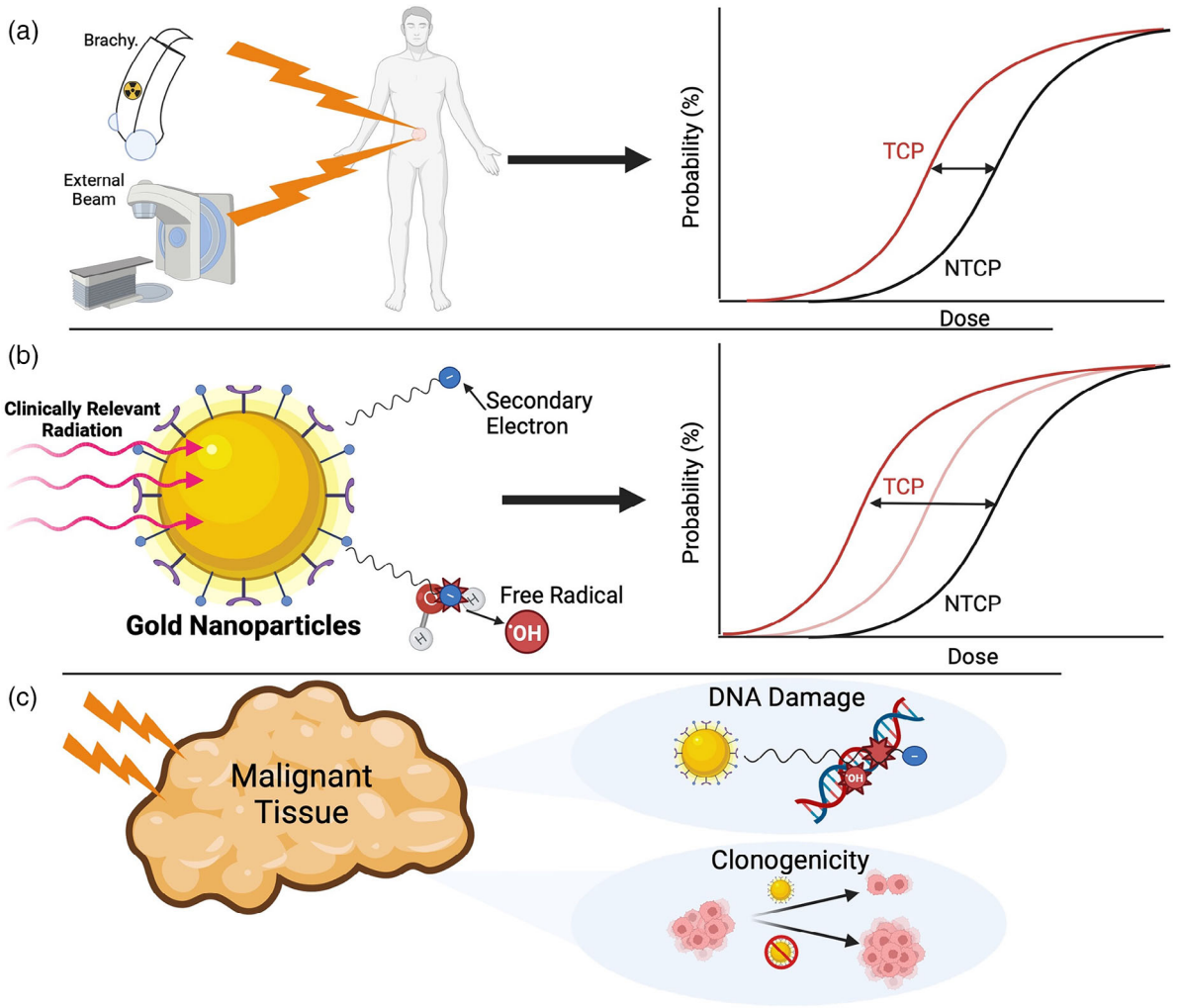

FIGURE 1 Radiation delivery with GNP radiosensitization. (a) Achieving optimal tumour control probability (TCP) is limited in current radiotherapy treatments (brachytherapy and external beam radiotherapy) via the associated normal tissue complication probability (NTCP). (b) GNP radiosensitization via the generation of secondary electrons and free radicals can improve the therapeutic index. (c) Cellular viability and damage from radiotherapy treatments and nanoparticle administration can be measured using DNA damage assays and cellular proliferation assays.

limited biologically relevant systems that cannot accurately simulate additional endogenous processes. Thus, there exists a gap in the current research surrounding GNPs + HDR-BT that can demonstrate their efficacy using relevant GNP concentrations on representative biological systems.

The goal of this study is to characterize GNP radiosensitization in vitro between clinically relevant radiation delivery methods from an HDR-BT source (192-Ir) and EBRT (6 MV LINAC). Effective characterization of nanotechnology radiosensitization is achieved through a comparison under variable irradiation conditions. It is hypothesized that the mechanism of action of GNPs varies between incident photon energies resulting in variable radiosensitization; however, it is unknown whether additional endogenous or extrinsic factors may affect the reported radiosensitization. By employing identical experimental parameters between photon delivery methods, a direct comparison of the dose enhancement achieved with GNPs from different treatment modalities is possible and can more effectively quantify the role GNPs play in radiosensitization. To achieve this, a novel Solid Water phantom was designed for in vitro irradiations from an HDR-BT afterloader and a 6 MV LINAC. Monolayer HeLa (cervical cancer) and PC3 (prostate cancer) cell cultures were incubated with 10 μg/mL concentration of GNPs and irradiated to a conventional fractionation scheme. Cell viability and survival were characterized using clonogenic and DNA double-strand break assays (Figure 1c). To the authors' knowledge, this is a first-of-its-kind in vitro study on the dose enhancement achieved with GNPs dosed at feasible concentrations from an HDR-BT source compared to MV irradiations. This work is a foundation for future studies evaluating the use of GNPs with HDR-BT radioactive sources.

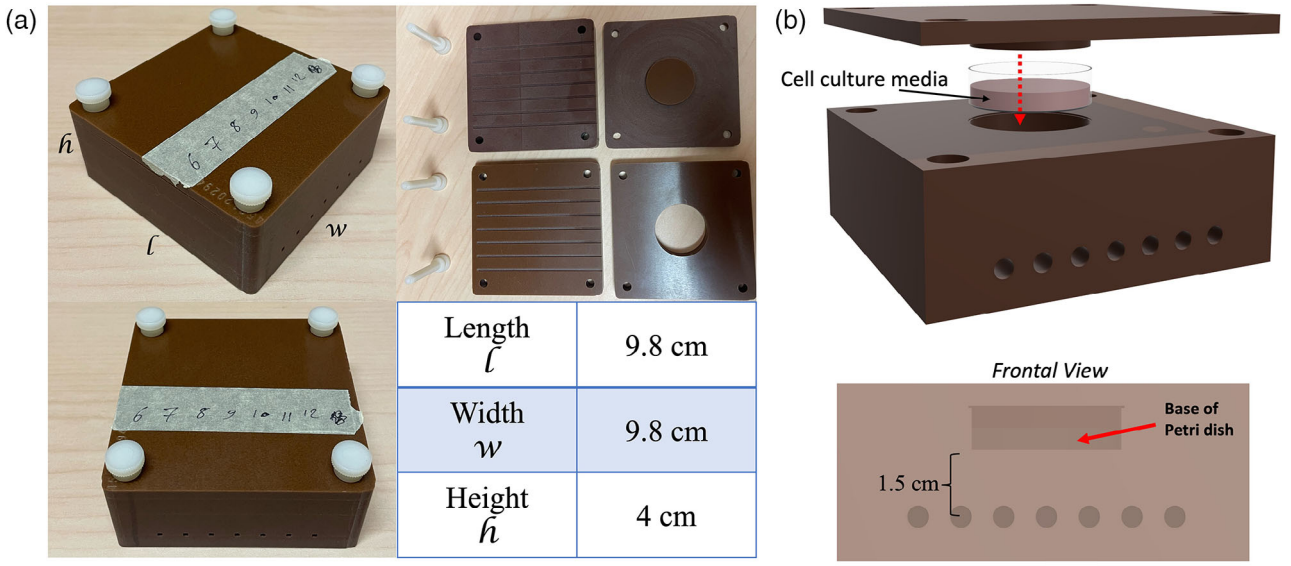

FIGURE 2 Solid Water Phantom for HDR Irradiations. (a) Phantom design and external dimensions. (b) CAD model of phantom showing insertion of Petri dish within the phantom.

2 | METHODS AND MATERIALS

2.1 | Phantom development

A 9.8 cm x 9.8 cm x 4 cm phantom was machined from existing Solid WaterTM (SW) blocks to encase a 35 mm Petri dish containing monolayer cell cultures at its base (Figure 2). The phantom was designed to ensure scattered photon equilibrium from a common HDR brachytherapy source (Flexisource Ir-192). Seven equally spaced needle insertion cavities were drilled 1.5 cm below the base of the petri dish and 1 cm apart. The cavities extended 9.4 cm into the SW, parallel to the base of the petri dish. A 0.5 cm protrusion extends from the lid to sit atop the cell culture during irradiations to limit air gaps. Holes for four plastic screws were drilled 0.5 cm from each edge of the phantom to fix the SW in place during irradiations. The diameter of the petri dish location was 3.65 cm, with a small lip carved at the top of the SW so the petri dish would be fixed in position.

2.1.1 | Film verification for high dose-rate treatment plan delivery

A petri dish was filled with tap water and placed in the phantom to mimic cell culture media. The phantom was CT scanned on a GE Healthcare CT Scanner (GE Healthcare, California, USA), and the DICOM file was then imported into Oncentra (Elekta Brachytherapy Solutions, Veenendaal, The Netherlands) treatment planning system (TPS) for HDR brachytherapy (Figure S1a). The base of the Petri dish was contoured as the planning target volume and set to the 100% isodose line for a 200 cGy dose prescription. Five of the seven needle insertions were selected for the calculated source dwell positions to generate a treatment plan. In total, 50 dwell positions were generated. The treatment delivery setup for in vitro irradiations is shown in Figure S1b, depicting needle insertion from the HDR afterloader in the treatment vault.

Radiochromic film measurements were performed before cell irradiations to verify dose delivery and uniformity from the HDR treatment plan. Film calibration was achieved using Gafchromic EBT-4 film (Lot #: 11212401) from Ashland Specialty Ingredients G.P. (Bridgewater, NJ, USA) and a calibration curve generated from the 192-Ir source, as recommended by Huang et al.[30] for low-dose irradiations. Film calibration treatment setup and methodology are described in the Supplemental Information. For treatment delivery verification, EBT-4 film was cut in a circle using a paper cutter to fit at the base of the Petri dish. An orientation mark was added in the top corner of the film. The film was submerged in tap water to limit air gaps and enclosed in the phantom. Twenty-four hours post-irradiation, the film was read in the red channel using an Epson Expression 10000XL (Epson, Suwa, Japan) and processed on FilmQA Pro v.7 (Ashland Inc., Wayne, New Jersey, USA).

2.2 | GNP synthesis and characterization

The GNPs in this study were synthesized following a citrate reduction method.[31] 28.82 mL of de-ionized water was vigorously mixed with 1.18 mL of 1% tetrachloroauric acid ($HAuCl_4$) and brought to a boil. Once boiling, 1.2 mL of tribasic sodium citrate was rapidly added to the solution and left to boil for 5 min, during

which time the solution changed to a dark ruby colour, confirming the creation of GNPs. After 5 min, the solution was left to come to room temperature. The GNPs within this study were functionalized at a 2:1 ratio with polyethylene glycol (PEG) and a peptide containing integrin binding domain RGD (NPs denoted as GNP-PEG-RGD). PEG improves NP stability within media and prevents aggregation,[32] while RGD enables preferential GNP uptake within malignant tumour cells by targeting the $\alpha_v\beta_3$ integrin overexpressed by cancer cells.[33] Characterization of the GNPs and GNP-PEG-RGD complex was achieved with transmission electron microscopy, ultraviolet-visible spectrometry, dynamic light scattering, and zeta potential analysis. The GNP-PEG-RGD complex will be referred to simply as GNPs for the remainder of the manuscript.

2.3 | Cell culture and GNP uptake

Human Prostate cancer cell line, PC-3 (ATCC#: CRL-1435™) and Cervical cancer cell line, HeLa (ATCC#: HBT-3), were purchased from the American Type Culture Centre (ATCC). Cells were cultured in T-75 flasks using high glucose Dulbecco's Modified Eagle medium (DMEM; Gibco) supplemented with 4 mM GlutaMax (Gibco), 10% Fetal Bovine Serum (Gibco) and 1% penicillin/streptomycin (Gibco). Washing of cell cultures was performed using phosphate-buffered saline (PBS), and TrypLE (Gibco) was used for cell detachment. Cells were incubated at 37°C with 5% CO_2 and subcultured every 3–5 days once ~80%–90% confluency was achieved.

Cell cultures plated in 35 mm Petri dishes were dosed with GNPs 24 h prior to irradiation experiments. The GNP dosing concentration was 10 μg/mL for all experiments. GNP uptake in the cellular membrane was verified using live-cell imaging, hyperspectral imaging (HIS), and inductively coupled plasma mass spectrometry (ICP-MS). For live-cell imaging, cells were plated on 35 mm coverslip bottom dishes (MatTek, Ashland, MA USA). After 24 h, cell cultures were dosed with a Cy5-thiol-PEG-labeled GNP complex at a concentration of 10 μg/mL. The GNP complex was previously shown to be stable via DLS and ζ-potential measurements.[14] Cell cultures were then incubated for 24 h, after which the media containing the GNPs was removed and replaced with fresh media. NucBlue Live ReadyProbes Reagent (R37605; ThermoFisher Scientific, Waltham, MA, USA) containing Hoechst 33,342 dye was used to stain nuclei before imaging. Images were taken using a 60 × oil immersion objective lens using a confocal laser scanning microscope (Zeiss LSM 980, Carl ZeissMicroscopy GmbH, Jena, Germany). Hyperspectral imaging (HSI) and darkfield imaging were performed to further characterize GNP uptake in cellular membranes. HSI is a useful imaging probe as it allows each imaging pixel to be related to a complete spectral response, characterizing NP presence. Due to the unique surface plasmon resonance properties of GNPs, they can be characterized using HSI. As a quantitative verification of GNP penetration into cells, inductively coupled plasma mass spectrometry (ICP-MS; Agilent 8800 Triple Quadrupole, Agilent Technologies, Santa Clara, CA, USA) was performed on GNP-incubated cells by comparing to gold-standard solutions of concentrations 1, 5, 10, and 50 ngAu/mL.

2.4 | In vitro cellular irradiations

Prior to irradiation, HeLa and PC3 cell cultures were seeded to the bottom of a 35 mm Petri dish at cell densities of 3.0×10^5 cells/mL and 4.0×10^5 cells/mL, respectively. 24 h after seeding, the cells were dosed with the GNP complex at a concentration of 10 μg/mL for 24 h. HDR in vitro radiation exposures were performed with an Elekta Flexitron HDR Afterloader (Model: 136149, Elekta, VEENENDAAL, Netherlands). Samples were encased within Solid Water in the HDR phantom, as described in Figure 2b. Dose delivery was accomplished with a 192-Ir source. For 200 cGy irradiations, the delivery took approximately 200 s, based on the then source activity of 7 Ci, corresponding to a dose rate of 0.67 Gy/min according to the treatment geometry. LINAC in vitro radiation treatments were performed with a clinical 6 MV linear accelerator (Varian Truebeam, Palo Alto, CA, USA). Samples were placed in the HDR phantom with the lateral SW extension to ensure photon scatter equilibrium at 6 MV (see Figure S2 for the LINAC treatment delivery setup). Samples were irradiated at a source-axis distance of 100 cm. A field size of 10 cm x 10 cm and a dose rate of 600 monitor units (MUs) per minute were used for all irradiations, delivering 220 MU for a final dose rate of 5.5 Gy/min. The appropriate number of MUs to administer was calculated using Eclipse 15.606 (Varian Medical Systems, Palo Alto, California, USA) after importing the CT-scanned phantom into the Eclipse treatment planning system. A commissioned AAA algorithm was then used to determine the required number of MUs to deliver 200 cGy to the target volume. Non-irradiated samples were transported along with irradiated samples to maintain consistency. After irradiations, cells were returned to the lab for sample prep and analysis.

2.5 | Clonogenic assay

Cells were seeded in a 35 mm Petri dish and incubated for 24 hrs, followed by the dosing procedure described in Section 2.4. After irradiation, cells were washed three times with PBS and trypsinized for cell counting. Fresh media was added to the Petri dishes to dilute the trypsin, and the cell suspension was transferred

to an autoclaved 1.5 mL Eppendorf tube. After cell counting, the required number of cells was transferred to a 15 mL test tube and serial diluted to seed 100 (0 Gy) or 300 (200 cGy irradiations, HDR/LINAC) cells in each plate. Cell cultures were left to incubate for 14 days for colony growth. After the incubation period, the media was poured out, and the cells were stained with 0.5% methylene blue for 10 min, after which the stain was washed with dH_2O and the plates were allowed to air-dry overnight. Using a 10X microscope, colonies were counted for plating efficiency (PE) and survival fraction (SF) statistics. PE was calculated by dividing the total number of colonies formed by the number of cells seeded; the SF was calculated by dividing the total number of colonies formed after irradiations by the number of cells seeded and dividing by the PE of the respective condition without irradiation. GNP-induced radiosensitization was evaluated by comparing the change in SF between GNP-incubated cells to control.

2.6 | DNA double-strand break assay

An immunofluorescent assay was used to probe DNA damage post-irradiation. Cells were seeded in 35 mm Petri dishes that contained glass coverslips at densities described in Section 2.4 and were incubated for 24 h. Dosing procedures also followed as described in Section 2.4. Post-irradiation, the media in each well was removed and replaced with fresh media before the cells were incubated. 24 h after irradiation, cells were washed three times using PBS and fixed with 4% paraformaldehyde (PFA). To assess the DNA double-strand breaks in cells, 53BP1, a protein involved in DNA repair pathways throughout the cell cycle,[34] was fluorescently labelled. This was accomplished using labelled antibodies against the repair protein. Cells were first dosed with 2% BSA/0.1% Triton-X in PBS and incubated for 20 min. The primary antibody solution was then diluted 1:200 using 0.5% BSA/0.1% Triton-X/PBS. The diluted solution was then placed on top of parafilm, and glass coverslips were placed face down onto the solution. Samples were left in a dark room to incubate for 1 h. Post-incubation, glass coverslips were washed twice with PBS and once with 0.5% BSA/0.1% Triton-X/PBS. The secondary antibody (Alexa Fluor 488) solution was diluted 1:500 with 0.5% BSA/0.1% Triton-X/PBS and placed onto parafilm. Coverslips were placed face down onto the solution and left to incubate for 30 min in a dark room at room temperature. Coverslips were again washed twice with PBS and mounted onto slides with ProLong (P36930; ThermoFisherScientific, Waltham, MA, USA) Glass Antifade Mountant for imaging. 53BP1 foci were imaged using a 60 × oil immersion lens using a confocal laser scanning microscope (Zeiss LSM 980). The secondary antibody used to fluorescently label the 53BP1 protein was tagged with Alexa Fluor 488 (excitation 490 nm, emission 525 nm). 53BP1 images were processed, and foci and nuclei were counted. The radiosensitization was defined as the ratio of the foci count per nucleus with GNPs to control.

2.7 | Statistics

For all experiments, measurements were performed in triplicate to attain statistical significance. Between samples and conditions, a one-tailed Student's *T*-test with equal variance was performed. Statistical significance was defined as $\alpha = 0.05$. Error bars are listed as $\pm 1\sigma$.

3 | RESULTS

3.1 | HDR dose delivery validation and uniformity

Shown in Figure 3 are film irradiation results of the 200 cGy treatment delivery from the 192-Ir source. Construction of EBT-4 film consists of an active layer of thickness 30 μm encased by two thin polyester films of 125 μm thickness each. Upon irradiation, a marker dye in the active layer polymerizes, shading the film proportionately to the delivered dose. The optical density of the film can then be read on a flatbed scanner and related to the delivered dose for calibration or plan verification.

Irradiated and non-irradiated film is shown in Figure 3b. The pixel values in the red, green, and blue channels are shown in Figure 3c, with the calibration doses given in the adjacent table. Lower doses, such as 10 and 20 cGy, were omitted from the 192-Ir calibration protocol as the corresponding dwell times were below the deliverable threshold of the treatment system. Across the face of the irradiated film, absolute dose delivery was within -5% and +10% of the expected 200 cGy treatment prescription, neglecting the orientation mark in the upper right of the film. Given dose heterogeneity in clinical HDR brachytherapy treatments can exceed 30%, a dose-delivery range of 15% is acceptable and is not expected to significantly affect cell viability measurements. Vertical and horizontal profiles of the irradiated film showed flatness and symmetry to within 5% of the central axis dose, demonstrating uniformity across the face of the petri dish.

3.2 | GNP characterization

The GNPs were functionalized with PEG and RGD to improve nanoparticle uptake within media. For this in vitro study, PEG was included considering the nanoparticle's translation in vivo, which shields the GNPs from opsonization, prolonging their blood circulation time.[32] While PEG-functionalized GNPs alone may

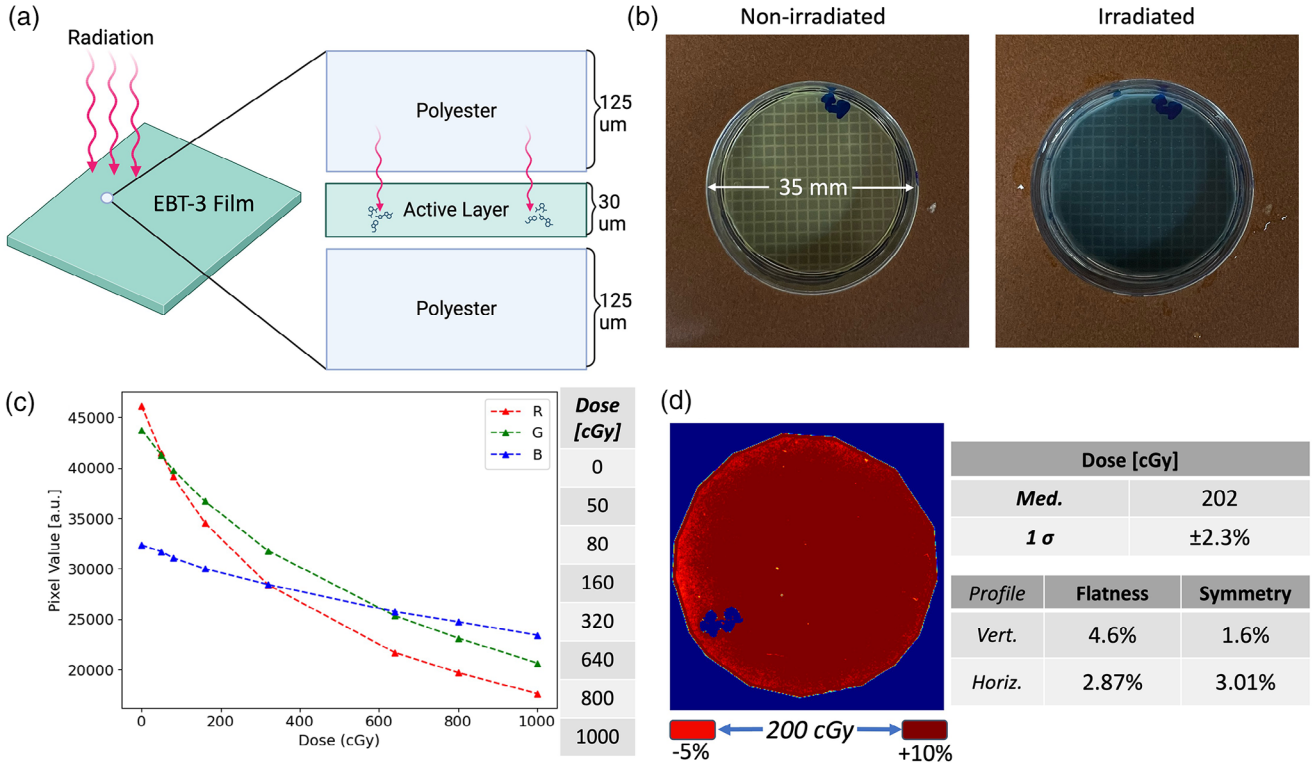

FIGURE 3 Measurement of irradiation via 192-Ir using EBT-4 film. (a) EBT-4 Film with active layer polymerizing from incident radiation. (b) Non-irradiated (Left) and irradiated (Right) EBT-4 film within base of the Petri dish. (c) Dose calibration curve from 192-Ir source from 0 cGy to 1000 cGy treatment prescriptions. (d) Dose map (Left) and horizontal and vertical profiles (Right) of irradiated film read in the red color channel.

demonstrate reduced intracellular uptake,[35] the addition of the RGD peptide enables preferential targeting of PC-3 and HeLa cells, which have been shown to express the $\alpha_v\beta_3$ integrin.[36,37]

Confirmation of GNP synthesis and functionalization was accomplished using transmission electron microscopy (TEM), ultraviolet-visible spectrometry (UV-Vis), dynamic light scattering (DLS), and zeta potential techniques (Figure S4). TEM images confirm the core diameter of the as-made citrate-capped GNPs at 12.8 nm ± 0.12 nm. From both DLS measurements, the addition of PEG and RGD to the surface of the bare GNPs increased the diameter of the nanoparticles. The addition of PEG and RGD red-shifted the spectra peaks of UV-VIS from 521.75 nm to 522.15 nm. The hydrodynamic diameter of the GNPs increased from 16.2 nm ± 0.2 nm to 24.2 nm ± 0.1 nm with the conjugation of PEG and RGD, with a polydispersity index of 18.0% ± 0.6% and 24.8% ± 0.3%, respectively. The ζ-potential of the bare GNPs and GNP-PEG-RGD complex was measured to be −37.95 mV± 0.31 mV and −4.66 mV± 0.29 mV, respectively. The recorded increase in the ζ-potential with the addition of PEG/RGD is due to the negatively charged citrate molecules being replaced by the neutral PEG and positively charged RGD peptides. The stability of the GNP-PEG-RGD complex in PBS and cell culture media DMEM has previously been demonstrated by Jackson et al.[38] and Bromma et al.[14]

3.3 | Intracellular GNP uptake

Figure 4 depicts intracellular nanoparticle uptake via receptor-mediated endocytosis. GNPs aggregate within intercellular media before the ligands on the surface of the GNPs (RGD) interact with cell-membrane receptors[39] (Figure 4a). The receptors binding to the GNPs cause membrane curvature, reducing configurational entropy and greater localization of receptors at the wrapping site, causing complete membrane wrapping around the nanoparticle. Live-cell imaging with a confocal microscope, inductively coupled plasma mass spectrometry (ICP-MS), and hyperspectral darkfield imaging (HSI) were performed to verify intracellular GNP uptake. Confocal images showing intracellular uptake of Cy5-labeled GNP complex are shown in Figure 4b. Qualitatively, GNP uptake is similar between both HeLa and PC3 cell lines. GNP aggregation is observed around the nucleus without penetration, given the size of the GNPs being larger than that of nuclei pores. HSI darkfield images are shown in Figure 4c, qualitatively confirming the presence of GNPs within the cellular membrane. ICP-MS experiments to quantitively verify GNP accumulation in the cellular membrane are shown in Figure 4d. Similar to that observed in Figure 4b, GNP uptake per cell is similar between both cell lines (HeLa: 8.7×10^5 GNPs/cell; PC3: 6.0×10^5 GNPs/cell), comparable to previously published results.[38,40] It should

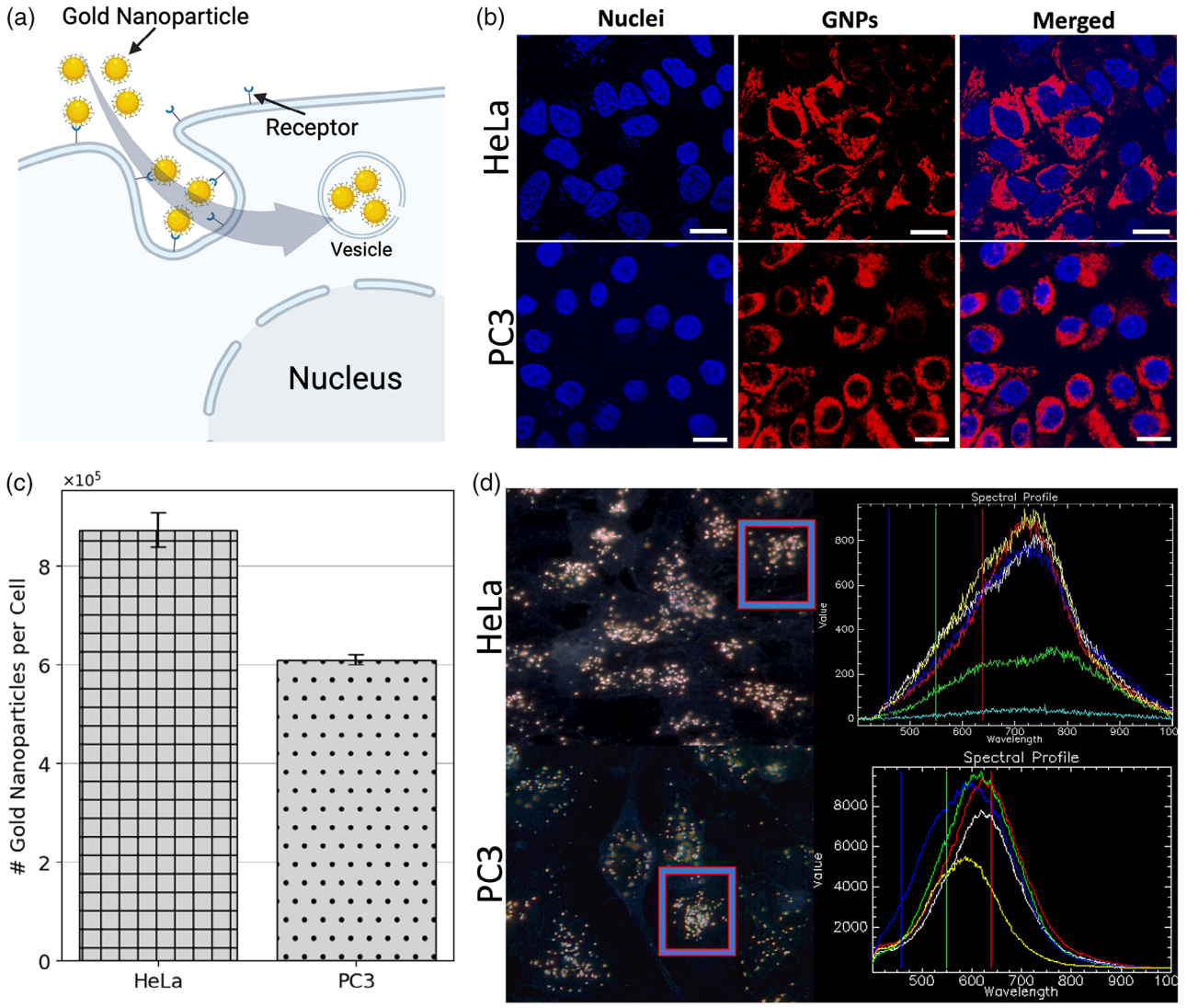

FIGURE 4 Intracellular GNP uptake. (a) Receptor-mediated endocytosis of GNPs. (b) Confocal images of DAPI stained nuclei (blue) and Cy5-labelled GNPs (red) from a dosing concentration of 10 μg/mL. (c) HSI of GNP accumulation in HeLa (left) and PC3 (right) cells with spectra collected from the GNPs. (d) Quantification of the number of GNPs within HeLa and PC3 cells. Scale bar is 20 μm.

be emphasized that this technique to quantify absolute gold content in cells cannot disassociate the number of GNPs that have been internalized within the cells from the number of GNPs that have adhered to the cellular membrane before internalization. However, in combination with the confocal and darkfield images (Figure 4b,d), it is presumed that a significantly greater fraction of the total number of GNPs are internalized within the cytoplasm rather than simply adhered to the membrane.

3.4 | In vitro cell viability

When applied to radiotherapy in vitro experiments, the clonogenic assay is an effective measure of treatment viability by quantifying the remaining viable cells post-irradiation or intervention in an exposed culture (Figure 5a). Figure 5b shows the PE and SF of HeLa and PC3 cells exposed to 200 cGy from HDR or LINAC irradiations. With no radiation exposure, GNPs did not significantly reduce the PE of the two cell lines, indicating no additional toxicity from the NPs, supported by previously published results.[38,41] Indeed, the decision to administer the chosen GNP concentration of 10 μg/mL is due to its feasibility for in vivo experiments that offer no cytotoxicity to the animals.[38] Significantly greater radiosensitization from GNPs with HDR irradiations was reported for both cell lines compared to LINAC irradiations. For HeLa cells, GNPs reduced the SF by an additional 4.9% ($p = 0.009$) and 2.4% ($p = 0.08$) for HDR and LINAC irradiations, respectively. For PC3 cells, GNPs reduced the SF by 8.6% ($p = 0.03$) and 1.9% ($p = 0.25$) for HDR and LINAC irradiations, respectively. HDR+GNP irradiations reduced cell survival by 4.6% ($p = 0.03$) and 8.5% ($p = 0.03$) compared to LINAC+GNP irradiations for HeLa and PC3 cells,

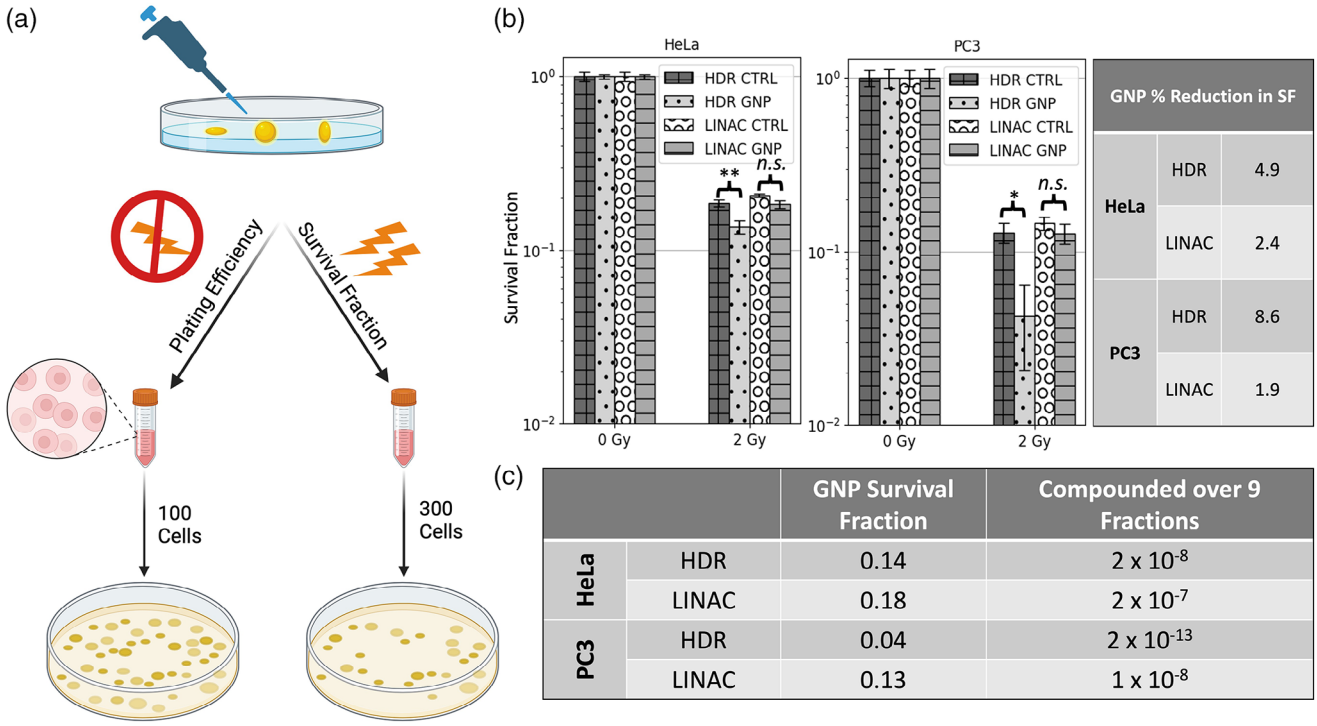

		GNP Survival Fraction	Compounded over 9 Fractions
HeLa	HDR	0.14	2×10^{-8}
	LINAC	0.18	2×10^{-7}
PC3	HDR	0.04	2×10^{-13}
	LINAC	0.13	1×10^{-8}

FIGURE 5 Colony formation post-irradiation. (a) Clonogenic assay protocol. (b) Survival fraction of HeLa (Left) and PC3 (Right) cells dose with and without GNPs. (c) Tumour control probability calculations after nine treatment fractions on a tumor volume containing 10^8 cells. *n.s.: not significant; *: $p < 0.05$; **: $p < 0.01$.*

respectively. As predicted, GNP-induced radiosensitization from the 192-Ir source is significantly greater than the 6 MV photon energy, potentially resulting from the increased photoelectric cross-section.

Furthering our cell viability analysis of GNP-induced radiosensitization, an immunohistochemistry-based assay was used to probe induced DNA damage with GNPs. This was accomplished by measuring the DSB foci per nuclei induced from the recruitment of 53BP1, a protein involved in DNA repair, which is then stained with fluorescent antibodies (Figure 6a). DNA DSB repair primarily occurs via nonhomologous end-joining (NHEJ) or homologous recombination repair (HRR). The 53BP1 protein signals NHEJ, which does not use a DNA template for replication and is generally regarded as error-prone compared to the counter HRR.[42] The irradiated and non-irradiated cells were fixed 24 h post-treatment to measure residual damage, which often goes unrepaired, leading to loss of clonogenic potential. Shown in Figure 6 are results from the employed immunohistochemistry DNA DSB assay. Figure 6b depicts confocal images showcasing nuclei (blue) and DSB foci (green) of HeLa cells under our irradiation conditions (see Figure S5 for confocal images of PC3 cells). Qualitatively, the number of foci per cell generally increases with the incorporation of GNPs (Figure 6b). Notably, GNPs did not elicit additional DNA damage with no incident radiation, confirming their non-cytotoxic nature as previously demonstrated by the clonogenic results. Indeed, the choice of GNP size restricts their permeation through the nuclear membrane, resulting in their distribution throughout the cytoplasm without penetration into the nucleus (Figure 4b).

Figure 6c reports averaged foci per nucleus from each irradiation condition. Significantly greater DNA damage occurred with HDR irradiations compared to LINAC irradiations under both conditions. From HDR+GNP irradiations, DNA damage was increased by 183% ($p < 0.001$) and 364% ($p = 0.01$) for HeLa and PC3 cells, respectively, compared to LINAC+GNP irradiations. GNPs induced significantly greater DNA damage for HeLa cells under both HDR ($p < 0.01$) and LINAC ($p < 0.001$) irradiations. For PC3 cells, GNPs induced greater damage under both irradiation conditions, but this effect was not significant with HDR-BT irradiations ($p > 0.05$).

4 | DISCUSSION

High dose rate brachytherapy may offer ideal conditions for implementing GNPs as radiosensitizing agents as compared to their implementation into conventional high-energy external beam radiotherapy. In this study, we compared GNP-induced radiosensitization of cervical and prostate cancer cell lines dosed with low concentrations of GNPs and irradiated via either an 192-Ir source or a 6 MV photon beam from a

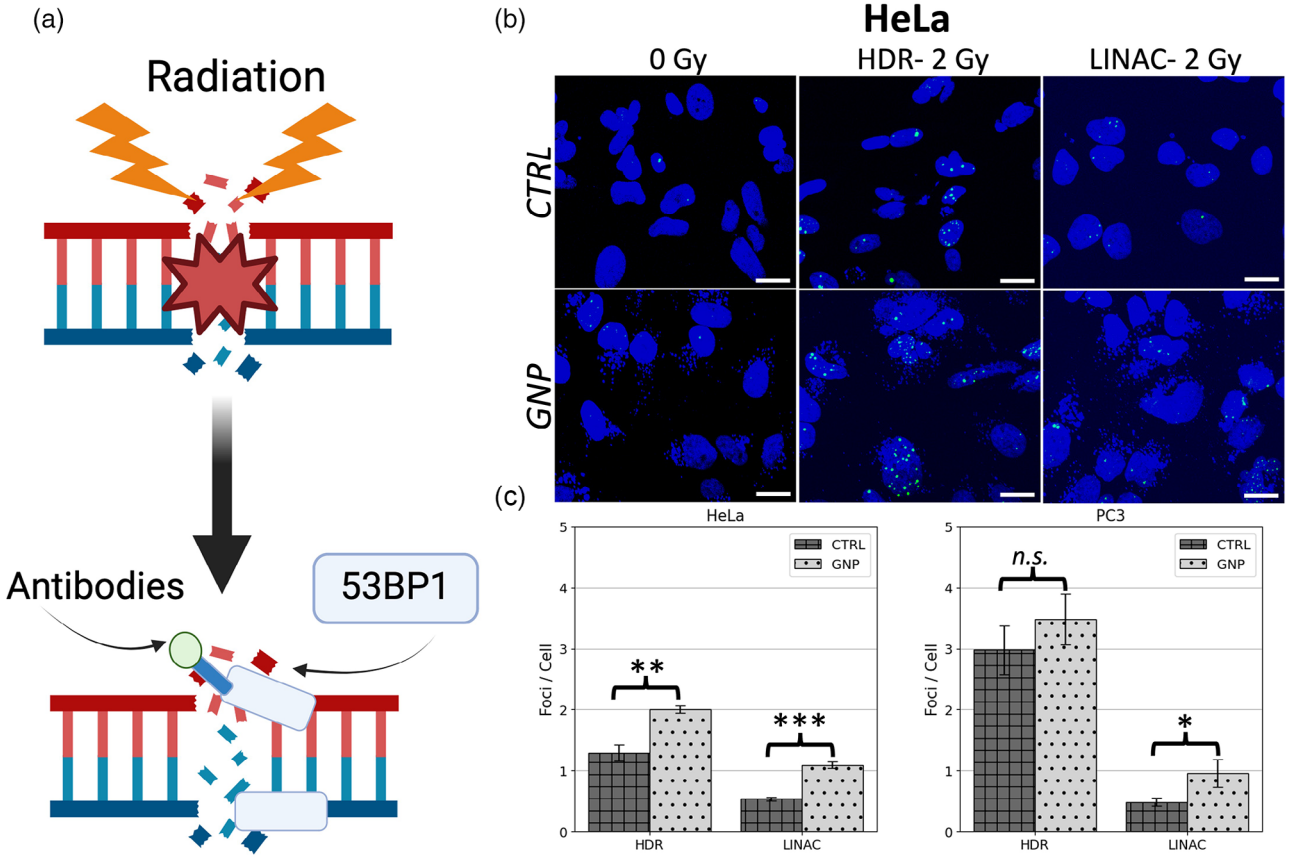

FIGURE 6 Radiation-induced DNA damage and fluorescent antibody staining of DNA repair proteins. (a) Fluorescent antibody staining post-radiation-induced DNA damage. (b) Confocal images of DAPI-stained nuclei (blue) and DNA damage (green) of HeLa (Left) and PC3 (Right) cells irradiated from either an HDR brachytherapy source or LINAC. (c) Averaged foci count per cell nuclei corrected for 0 Gy 24 h post-irradiations for HeLa (left) and PC3 (right) cells. Scale bar is 20 μm. *n.s.: not significant; *: $p < 0.05$; **: $p < 0.01$; ***: $p < 0.001$.*

clinical LINAC. By comparing loss in clonogenic potential and increased DNA damage, the radiosensitizing properties of 12 nm spherical GNPs can be further elucidated.

The optimal dosing strategy is important to ensure limited toxicity from the GNPs in vitro and in vivo as well as inducing sufficient radiosensitization. MC studies demonstrate that significantly large gold concentrations above 1 g Au / kg tissue are required, though these high concentrations may not translate clinically due to toxicity concerns in vivo. Lower concentrations, such as those administered in this study, have also shown sufficient radiosensitization, demonstrating that high concentrations may not be required as recommended by MC studies.[27–29] The 10 μg/mL dosing concentration here, approximately translates to 2 mg/kg in vivo, well below the LD_{50} of GNPs reported for mice.[43] Therefore, this dosing concentration could be clinically feasible in future efficacy and clinical studies; however, a thorough investigation into their prolonged toxicity at this concentration should be conducted, as it has previously been shown that administered GNPs in vivo reside in organs for prolonged periods of time.[44,45]

Ensuring accurate and reproducible treatment delivery during HDR-BT irradiations was verified before in vitro irradiations. We used EBT-4 radiochromic film to determine the median dose delivery to the base of a Petri dish along with its flatness and symmetry in the horizontal and vertical profiles. Film calibration was performed using a calibration curve generated from the 192-Ir source. Conventionally, a 6 MV calibration curve is generated for use with future radiochromic film measurements, as EBT-4 film is effectively energy-independent in the higher-energy range.[46] However, as Huang et al.[30] discuss, for 192-Ir irradiations, they recommend generating a 192-Ir calibration curve for doses < 250 cGy. Therefore, we chose to calibrate the EBT-4 film using a 192-Ir calibration curve.

GNP-induced radiosensitization, measured via increased DNA damage, was larger after LINAC irradiations for both cell lines. DSB foci per cell increased by 102% and 99% for LINAC irradiations compared to only 93% and 17% from HDR irradiations for HeLa and PC3 cells, respectively. This result did not correlate with that found from the clonogenic assay that suggested GNPs elicit greater dose enhancement with kV than MV

photon sources.[12,15,47] With the substantially greater DNA damage observed from HDR irradiations without GNPs relative to LINAC irradiations for both cell lines, any effective GNP-induced radiosensitization may be unable to be measured with the current assay technique. Given the current technique requires observation of the fluorescent foci in the nuclei, an accurate measurement of GNP radiosensitization may be impaired via the saturation of DNA damage seen in Figures 6 and S4.

Given that significantly greater radiosensitization was reported via our clonogenic assay, we may hypothesize that DNA damage may not be the only factor when considering GNP-radiosensitization. Other contributors reported in the literature are mitochondrial damage and ROS generation leading to oxidative stress, both of which may be augmented with GNPs.[38,48–51] GNPs have been shown to disrupt the mitochondrial membrane potential and oxidation, resulting in apoptosis and greater cell-damaging species.[52] In addition, GNPs have been observed to produce hydroxyl radicals through the dismutation of mitochondrial superoxide, which may be increased via radiation-induced effects, leading to a greater concentration of ROS. Future work characterizing GNP radiosensitization from HDR irradiations will explore both damage incurred to mitochondria in the cells and the proportional ROS generation.

The dose rate of the incoming radiation has been shown to affect GNP-induced radiosensitization. In the present study, 200 cGy irradiations were delivered from a LINAC at a dose rate of 600 MU/min, corresponding to a dose rate of 5.5 Gy/min. At the apparent activity level of 7 Ci, the HDR treatment was delivered over 3 min, corresponding to a dose rate of 0.67 Gy/min, significantly lower than that from the LINAC. Morozov *et al.*[7] studied the relative dose enhancement from spherical GNPs at varying sizes and dose rates irradiated to 500 cGy from a 200 kVp source. The authors found that at sizes below 20 nm, there was a 1.13-fold increase in dose enhancement between dose rates of 0.2 Gy/min and 2.1 Gy/min. Other studies have similarly reported a dose-rate dependence on GNP dose enhancement. Marques et al.[53] reported that higher dose rates induced greater genomic instability in PC3 cells incubated with thiolated GNPs. One potential explanation for the apparent dose-rate dependence is ROS generation. At higher dose rates, the generation of ROS may outpace the rate of ROS scavengers, leading to greater cellular damage, which may explain the greater radiosensitization properties observed with LINAC irradiations from our DNA damage assay. However, as demonstrated with the clonogenic assay, GNP radiosensitization with the 192-Ir was significantly greater compared to the LINAC irradiations, indicating a multifaceted mechanism behind GNP-induced radiosensitization. With HDR brachytherapy, whose dose rate depends on the strength of the source at the time of treatment, GNP-induced radiosensitization may differ to a significant extent over the lifetime of the source. Therefore, further clarification of the GNP dose rate dependency is required to characterize the radiosensitization properties of GNPs effectively.

The apparent GNP-induced radiosensitization properties reported in our study from LINAC irradiations align with previous research.[49] Compared to MC studies, our measured radiosensitization is larger than predicted at similar GNP concentrations, which further supports the conclusion that the mechanism of action of GNPs is multi-faceted, and not solely reliant on photoelectrons.[27,54] Other in vitro 192-Ir studies employing GNPs report significant radiosensitization, similar to that reported here.[24,25] However, as discussed previously, these studies either employed higher GNP concentrations (0.197 mg/mL) or used cultures of DNA that do not incorporate other endogenous processes in a cell. As we have shown above, DNA damage in the nuclei of functioning cells may not accurately represent the radiosensitization properties of GNPs. In addition, we have shown effective radiosensitization in vitro using monolayer cell cultures that have been incubated with clinically achievable concentrations of GNPs. The functionalization of our GNPs also allows for effective targeting of malignant tissue in vitro and in vivo,[38] not found in other studies. Shahhoseini et al. used 15 nm GNPs stabilized with a highly water-soluble organic shell with no apparent additional targeting functionalization, limiting tumour-specific uptake. Similarly, Yogo et al. used positively and negatively charged GNPs to target DNA in solution, though it is currently unknown whether additional targeting moieties could be effective in achieving tumour penetration and retention. While past research on the incorporation of GNPs into HDR brachytherapy offers effective demonstrations of their use in vitro, the novelty of our work enables future research with low, non-toxic concentrations of targeted and stable GNPs.

5 | CONCLUSIONS

Normal tissue toxicity currently limits effective dose escalation in radiotherapy to achieve nominal tumour control. High-Z nanoparticles can achieve the required dose enhancement by preferentially increasing the photoelectric cross-section in malignant tissue. Their characterization in separate treatment modalities and cancer phenotypes is mandatory for their successful implementation into treatment workflows. Given the high-Z nature of GNPs, it is hypothesized that dose enhancement should be greater at lower photon energies. In this research, we employed clinically relevant GNP sizes and concentrations to characterize the differential response from GNPs in cell viability between an 192-Ir HDR-BT source and 6 MV LINAC. HDR+GNP irradiations elicited 183% and 364% greater DNA

damage and 4.6% and 8.5% reduction in the SF of HeLa and PC3 cells, respectively, compared to LINAC+GNP irradiations. Given the known radiosensitization properties of GNPs and the results reported in this study, further in vitro and in vivo research is warranted to characterize GNP-induced radiosensitization with HDR-BT for their effective clinical translation into current treatments.

ACKNOWLEDGMENTS

The authors would like to thank the contributions of Dr Kyle Bromma for his assistance with radiochromic film calibrations. This research was funded by a NanoMedicines Innovation Network (NMIN) Strategic Initiative (SI) grant,2021-RES-SI-05; Natural Sciences and Engineering Research Council (NSERC) Discovery Grant (DG), RGPIN-2017-04501; Canadian Institutes of Health Research grant, DC0190GP.

CONFLICT OF INTEREST STATEMENT

The authors declare no conflicts of interest.

CONSENT FOR PUBLICATION

Not applicable.

DATA AVAILABILITY STATEMENT

The datasets used and/or analyzed during the current study are available from the corresponding author on reasonable request-

REFERENCES

1. Zhou R, Zhao D, Beeraka NM, et al. Novel Implications of Nanoparticle-Enhanced Radiotherapy and Brachytherapy: Z-Effect and Tumor Hypoxia. *Metabolites*. 2022;12(10):943. doi:10.3390/metabo12100943
2. Verry C, Dufort S, Villa J, et al. Theranostic AGuIX Nanoparticles as Radiosensitizer: A Phase I, Dose-Escalation Study in Patients with Multiple Brain Metastases (NANO-RAD Trial). *Radiother Oncol*. 2021;160:159–165. doi:10.1016/j.radonc.2021.04.021
3. Chuang YC, Wu PH, Shen YA, et al. Recent Advances in Metal-Based NanoEnhancers for Particle Therapy. *Nanomaterials*. 2023;13(6):1011. doi:10.3390/nano13061011
4. Kim SR, Kim EH. Gold Nanoparticles as Dose-Enhancement Agent for Kilovoltage X-Ray Therapy of Melanoma. *Int J Radiat Biol*. 2017;93(5):517–526. doi:10.1080/09553002.2017.1276309
5. Boateng F, Ngwa W. Delivery of Nanoparticle-Based Radiosensitizers for Radiotherapy Applications. *Int J Mol Sci*. 2020;21(1):273. doi:10.3390/ijms21010273
6. Lo CY, Tsai SW, Niu H, et al. Gold-Nanoparticles-Enhanced Production of Reactive Oxygen Species in Cells at Spread-Out Bragg Peak under Proton Beam Radiation. *ACS Omega*. 2023;8(20):17922–17931.
7. Morozov KV, Kolyvanova MA, Kartseva ME, et al. Radiosensitization by Gold Nanoparticles: Impact of the Size, Dose Rate, and Photon Energy. *Nanomaterials* 2020;10(5):952. doi:10.3390/nano10050952
8. Bromma K, Chithrani DB. Advances in Gold Nanoparticle-Based Combined Cancer Therapy. *Nanomaterials* 2020;10(9):1–25. doi:10.3390/nano10091671
9. Schuemann J, Berbeco R, Chithrani DB, et al. Roadmap to Clinical Use of Gold Nanoparticles for Radiation Sensitization. *Int J Radiat Oncol Biol Phys*. 2016;94(1):189–205. doi:10.1016/j.ijrobp.2015.09.032
10. Tudda A, Donzelli E, Nicolini G, et al. Breast Radiotherapy with Kilovoltage Photons and Gold Nanoparticles as Radiosensitizer: An in Vitro Study. *Med Phys*. 2022;49(1):568–578. doi:10.1002/mp.15348
11. Mesbahi A, Jamali F, Gharehaghaji N. Effect of Photon Beam Energy, Gold Nanoparticle Size and Concentration on the Dose Enhancement in Radiation Therapy. *BioImpacts*. 2013;3(1):29–35. doi:10.5681/bi.2013.002
12. Lin Y, McMahon SJ, Scarpelli M, Paganetti H, Schuemann J. Comparing Gold Nano-Particle Enhanced Radiotherapy with Protons, Megavoltage Photons and Kilovoltage Photons: A Monte Carlo Simulation. *Phys Med Biol*. 2014;59:7675–7689. doi:10.1088/0031-9155/59/24/7675
13. Zheng XJ, Chow JCL. Radiation Dose Enhancement in Skin Therapy with Nanoparticle Addition: A Monte Carlo Study on Kilovoltage Photon and Megavoltage Electron Beams. *World J Radiol*. 2017;9(2):63. doi:10.4329/WJR.V9.I2.63
14. Bromma K, Cicon L, Beckham W, Chithrani DB. Gold Nanoparticle Mediated Radiation Response among Key Cell Components of the Tumour Microenvironment for the Advancement of Cancer Nanotechnology. *Sci Rep*. 2020;10(1):12096. doi:10.1038/s41598-020-68994-0
15. Leung MKK, Chow JCL, Chithrani BD, Lee MJG, Oms B, Jaffray DA. Irradiation of Gold Nanoparticles by X-Rays: Monte Carlo Simulation of Dose Enhancements and the Spatial Properties of the Secondary Electrons Production. *Med Phys*. 2011;38(2):624–631. doi:10.1118/1.3539623
16. Sheeraz Z, Chow JCL. Evaluation of Dose Enhancement with Gold Nanoparticles in Kilovoltage Radiotherapy Using the New EGS Geometry Library in Monte Carlo Simulation. *AIMS Biophys*. 2021;8(4):337–345. doi:10.3934/BIOPHY.2021027
17. Martinov MP, Fletcher EM, Thomson RM. Multiscale Monte Carlo Simulations of Gold Nanoparticle Dose-Enhanced Radiotherapy II. Cellular Dose Enhancement within Macroscopic Tumor Models. *Med Phys*. 2023;50(9):5842–5852. doi:10.1002/mp.16460
18. Martinov MP, Fletcher EM, Thomson RM. Multiscale Monte Carlo Simulations of Gold Nanoparticle Dose-Enhanced Radiotherapy I: Cellular Dose Enhancement in Microscopic Models. *Med Phys*. 2023;50(9):5853–5864. doi:10.1002/mp.16454
19. Khoo AM, Cho SH, Reynoso FJ, et al. Radiosensitization of Prostate Cancers in Vitro and in Vivo to Erbium-Filtered Orthovoltage X-Rays Using Actively Targeted Gold Nanoparticles. *Sci Rep*. 2017;7(1):18044. doi:10.1038/s41598-017-18304-y
20. Kim SR, Kim EH. Feasibility Study on the Use of Gold Nanoparticles in Fractionated Kilovoltage X-Ray Treatment of Melanoma. *Int J Radiat Biol*. 2018;94(1):8–16. doi:10.1080/09553002.2018.1393579
21. Kiseleva M, Lescot T, Selivanova SV, Fortin MA. Gold-Enhanced Brachytherapy by a Nanoparticle-Releasing Hydrogel and 3D-Printed Subcutaneous Radioactive Implant Approach. *Adv Healthc Mater*. 2023;12(23):e2300305. doi:10.1002/adhm.202300305
22. Laprise-Pelletier M, Lagueux J, Côté MF, LaGrange T, Fortin MA. Low-Dose Prostate Cancer Brachytherapy with Radioactive Palladium–Gold Nanoparticles. *Adv Healthc Mater*. 2017;6(4):1601120. doi:10.1002/adhm.201601120
23. Ngwa W, Korideck H, Kassis AI, et al. In Vitro Radiosensitization by Gold Nanoparticles during Continuous Low-Dose-Rate Gamma Irradiation with I-125 Brachytherapy Seeds. *Nanomedicine Nanotechnology, Biol Med*. 2013;9(1):25–27. doi:10.1016/j.nano.2012.09.001
24. Shahhoseini E, Ramachandran P, Patterson WR, Geso M. Determination of Dose Enhancement Caused by AuNPs with Xoft® Axxent® Electronic (EBx^{TM}) and Conventional Brachytherapy: In Vitro Study. *Int J Nanomedicine*. 2018;13:5733–5741. doi:10.2147/IJN.S174624

25. Yogo K, Misawa M, Shimizu M, et al. Effect of Gold Nanoparticle Radiosensitization on Plasmid DNA Damage Induced by High-Dose-Rate Brachytherapy. *Int J Nanomedicine*. 2021;16:359–370. doi:10.2147/IJN.S292105
26. Alizadeh M, Ghorbani M, Haghparast A, Zare N, Ahmadi Moghaddas T. A Monte Carlo Study on Dose Distribution Evaluation of Flexisource 192Ir Brachytherapy Source. *Reports Pract Oncol Radiother*. 2015;20(3):204–209. doi:10.1016/j.rpor.2015.01.006
27. Gray T, Bassiri N, David S, et al. A Detailed Monte Carlo Evaluation of 192Ir Dose Enhancement for Gold Nanoparticles and Comparison with Experimentally Measured Dose Enhancements. *Phys Med Biol*. 2020;65(13)135007. doi:10.1088/1361-6560/ab9502
28. Ghorbani M, Bakhshabadi M, Pakravan D, Meigooni AS. Dose Enhancement in Brachytherapy in the Presence of Gold Nanoparticles: A Monte Carlo Study on the Size of Gold Nanoparticles and Method of Modelling. *Nukleonika*. 2012;57(3):401–406.
29. Lechtman E, Chattopadhyay N, Cai Z, Mashouf S, Reilly R, Pignol JP. Implications on Clinical Scenario of Gold Nanoparticle Radiosensitization in Regards to Photon Energy, Nanoparticle Size, Concentration and Location. *Phys Med Biol*. 2011;56(15):4631–4647. doi:10.1088/0031-9155/56/15/001
30. Huang L, Gaballa H, Chang J. Evaluating Dosimetric Accuracy of the 6 MV Calibration on EBT3 Film in the Use of Ir-192 High Dose Rate Brachytherapy. *J Appl Clin Med Phys*. 2022;23(5), e13571. doi:10.1002/acm2.13571
31. Li C, Li D, Wan G, Xu J, Hou W. Facile Synthesis of Concentrated Gold Nanoparticles with Low Size-Distribution in Water: Temperature and PH Controls. *Nanoscale Res Lett*. 2011;6(1):1–10. doi:10.1186/1556-276X-6-440/FIGURES/6
32. Suk JS, Xu Q, Kim N, Hanes J, Ensign LM. PEGylation as a Strategy for Improving Nanoparticle-Based Drug and Gene Delivery. *Adv Drug Deliv Rev*. 2016;99(Pt A):28–51. doi:10.1016/j.addr.2015.09.012
33. Garanger E, Boturyn D, Coll JL, Favrot MC, Dumy P. Multivalent RGD Synthetic Peptides as Potent Avβ 3 Integrin Ligands. *Org Biomol Chem*. 2006;4(10), 1958–1965. doi:10.1039/b517706e
34. Shibata A, Jeggo PA. Roles for 53BP1 in the Repair of Radiation-Induced DNA Double Strand Breaks. *DNA Repair (Amst)*. 2020;93:102915. doi:10.1016/j.dnarep.2020.102915
35. Cruje C, Chithrani BD. Integration of Peptides for Enhanced Uptake of PEGylayed Gold Nanoparticles. *J Nanosci Nanotechnol*. 2015;15(3):2125–2131. doi:10.1166/JNN.2015.10321
36. Liu Y, Zhao F, Gu W, et al. The Roles of Platelet GPIIb/IIIa and Alphavbeta3 Integrins during HeLa Cells Adhesion, Migration, and Invasion to Monolayer Endothelium under Static and Dynamic Shear Flow. *J Biomed Biotechnol*. 2009;2009:829243. doi:10.1155/2009/829243
37. Taylor RM, Severns V, Brown DC, Bisoffi M, Sillerud LO. Prostate Cancer Targeting Motifs: Expression of A$\nu\beta$3, Neurotensin Receptor 1, Prostate Specific Membrane Antigen, and Prostate Stem Cell Antigen in Human Prostate Cancer Cell Lines and Xenografts. *Prostate* 2012;72(5):523. doi:10.1002/PROS.21454
38. Jackson N, Hill I, Alhussan A, et al. Dual Enhancement in the Radiosensitivity of Prostate Cancer through Nanoparticles and Chemotherapeutics. *Cancer Nanotechnol*. 2023;14(1):75. doi:10.1186/s12645-023-00228-0
39. Chithrani DB. Intracellular Uptake, Transport, and Processing of Gold Nanostructures. *Mol Membr Biol*. 2010;27(7):299–311. doi:10.3109/09687688.2010.507787
40. Bromma K, Dos Santos N, Barta I, et al. Enhancing Nanoparticle Accumulation in Two Dimensional, Three Dimensional, and Xenograft Mouse Cancer Cell Models in the Presence of Docetaxel. *Sci Rep*. 2022;12(1):1–14. doi:10.1038/s41598-022-17752-5
41. Alhussan A, Bromma K, Perez MM, et al. Docetaxel-Mediated Uptake and Retention of Gold Nanoparticles in Tumor Cells and in Cancer-Associated Fibroblasts. *Cancers (Basel)*. 2021;13(13):3157. doi:10.3390/cancers13133157
42. Rodgers K, Mcvey M. Error-Prone Repair of DNA Double-Strand Breaks. *J Cell Physiol*. 2016;231(1):15-24. doi:10.1002/jcp.25053
43. Hainfeld JF, Slatkin DN, Smilowitz HM. The Use of Gold Nanoparticles to Enhance Radiotherapy in Mice. *Phys Med Biol*. 2004;49(18):309–315. doi:10.1088/0031-9155/49/18/N03
44. Zhang XD, Wu HY, Wu D, et al. Toxicologic Effects of Gold Nanoparticles in Vivo by Different Administration Routes. *Int J Nanomedicine*. 2010;5(1):771–781. doi:10.2147/IJN.S8428
45. Cho WS, Cho M, Jeong J, et al. Size-Dependent Tissue Kinetics of PEG-Coated Gold Nanoparticles. *Toxicol Appl Pharmacol*. 2010;245(1):116–123. doi:10.1016/j.taap.2010.02.013
46. Chan MF, Park J, Aydin R, Lim SB. Energy Dependence of the Gafchromic EBT4 Film: Dose-Response Curves for 70 KV, 6 MV, 6 MV FFF, 10 MV FFF, and 15 MV x-Ray Beams. *Med Phys*. 2023;50(6):3738–3745. doi:10.1002/mp.16240
47. Kirkby C, Ghasroddashti E. Targeting Mitochondria in Cancer Cells Using Gold Nanoparticle-Enhanced Radiotherapy: A Monte Carlo Study. *Med Phys*. 2015;42(2):1119–1128. doi:10.1118/1.4906192
48. Tabatabaie F, Franich R, Feltis B, Geso M. Oxidative Damage to Mitochondria Enhanced by Ionising Radiation and Gold Nanoparticles in Cancer Cells. *Int J Mol Sci*. 2022;23(13):6887. doi:10.3390/ijms23136887
49. Bromma K, Beckham W, Chithrani DB. Utilizing Two-Dimensional Monolayer and Three-Dimensional Spheroids to Enhance Radiotherapeutic Potential by Combining Gold Nanoparticles and Docetaxel. *Cancer Nanotechnol*. 2023;14(1):80. doi:10.1186/s12645-023-00231-5
50. Wolfe T, Chatterjee D, Lee J, et al. Targeted Gold Nanoparticles Enhance Sensitization of Prostate Tumors to Megavoltage Radiation Therapy in Vivo. *Nanomedicine Nanotechnology, Biol Med*. 2015;11:1277–1283. doi:10.1016/j.nano.2014.12.016
51. Chen Y, Yang J, Fu S, Wu J. Gold Nanoparticles as Radiosensitizers in Cancer Radiotherapy. *Int J Nanomed*. 2020;15:9407–9430. doi:10.2147/IJN.S272902
52. Taggart LE, McMahon SJ, Currell FJ, Prise KM, Butterworth KT. The Role of Mitochondrial Function in Gold Nanoparticle Mediated Radiosensitisation. *Cancer Nanotechnol*. 2014;5(1):1–12. doi:10.1186/s12645-014-0005-7
53. Marques A, Belchior A, Silva F, et al. Dose Rate Effects on the Selective Radiosensitization of Prostate Cells by GRPR-Targeted Gold Nanoparticles. *Int J Mol Sci*. 2022;23(9):5279. doi:10.3390/ijms23095279
54. Al-Musywel HA, Laref A. Effect of Gold Nanoparticles on Radiation Doses in Tumor Treatment: A Monte Carlo Study. *Lasers Med Sci*. 2017;32(9):2073–2080. doi:10.1007/s10103-017-2329-0

SUPPORTING INFORMATION

Additional supporting information can be found online in the Supporting Information section at the end of this article.

How to cite this article: Cecchi D, Jackson N, Goharian M, Beckham W, Chithrani D. Radiotherapeutic efficacy of gold nanoparticles for high dose-rate brachytherapy compared to conventional radiotherapy: An in vitro study. *Med Phys*. 2025;52:e18006. https://doi.org/10.1002/mp.18006